Detailing organelle division and segregation in *Plasmodium falciparum*

Julie M.J. Verhoef[1], Cas Boshoven[1], Felix Evers[1], Laura J. Akkerman[1], Barend C.A. Gijsbrechts[1], Marga van de Vegte-Bolmer[1], Geert-Jan van Gemert[1], Akhil B. Vaidya[2], Taco W.A. Kooij[1*]

[1]Department of Medical Microbiology, Radboudumc Center for Infectious Diseases, Radboud University Medical Center, Nijmegen, The Netherlands
[2]Center for Molecular Parasitology, Institute for Molecular Medicine and Infectious Disease, Department of Microbiology and Immunology, Drexel University College of Medicine, Philadelphia, USA

*Corresponding author: Taco.Kooij@radboudumc.nl

Abstract

The malaria causing parasite, *P. falciparum*, replicates through a tightly orchestrated process termed schizogony, where approximately 32 daughter parasites are formed in a single infected red blood cell and thousands of daughter cells in mosquito- or liver-stages. One-per-cell organelles, such as the mitochondrion and apicoplast, need to be properly divided and segregated to ensure a complete set of organelles per daughter parasites. Although this is highly essential, details about the processes and mechanisms involved remain unknown. We developed a new reporter parasite line that allows visualization of the mitochondrion in blood- and mosquito stages. Using high-resolution 3D-imaging, we found that the mitochondrion orients in a cartwheel structure, prior to stepwise, non-geometric division during the last stage of schizogony. Analysis of focused ion beam scanning electron microscopy (FIB-SEM) data confirmed these mitochondrial division stages. Furthermore, these data allowed us to elucidate apicoplast division steps, highlighted its close association with the mitochondrion, and showed putative roles of the centriolar plaques (CPs) in apicoplast segregation. These observations form the foundation for a new detailed model of mitochondrial and apicoplast division and segregation during *P. falciparum* schizogony and pave the way for future studies into the mechanisms of organelle division and segregation.

Introduction

Malaria is a devastating parasitic disease causing 247 million cases resulting in 619,000 deaths in 2021, especially in children under 5 years old[1]. *Plasmodium falciparum* is the most virulent parasite species causing malaria. Continued emergence of resistant parasites to antimalarial drugs is a major problem for global malaria control and necessitates continued development of novel antimalarials.

The malaria parasite harbors a unique mitochondrion that differs greatly from its host mitochondrion at a molecular and functional level[2]. While the most prominent role of the mitochondrion in humans is respiration and consequent energy conversion, in the disease-causing asexual blood-stages of *P. falciparum* the respiratory chain appears to be exclusively essential to support pyrimidine biosynthesis[3]. It is only during preparation for transition to the mosquito vector where sexual reproduction takes place, that canonical mitochondrial functions such as the tricarboxylic acid cycle (TCA) cycle and the oxidative phosphorylation (OXPHOS) pathway become more abundant and critical[4,5]. Because of these differences, it is not surprising that this organelle is the drug target of several anti-malarial compounds, such as atovaquone, DSM265, proguanil and ELQ300[6,7].

Host and stage transitions are commonplace in the complicated life cycle of *Plasmodium* parasites. During erythrocytic asexual replication, one parasite is segmented into approximately 32 merozoites through a tightly orchestrated process called schizogony. Schizogony happens on a much larger scale in mosquito and liver stages, where one parasite is divided into thousands or even tens of thousands of daughter parasites. *P. falciparum* harbors only a single mitochondrion during these stages, which needs to be properly divided and distributed among the daughter cells[8]. During parasite development in asexual blood stages, the tubular mitochondrion elongates and forms a large, branched network that stretches throughout the parasite[9]. Only during the final stages of schizogony, once nuclear division is completed, does the mitochondrion undergo rapid fission[10]. The apicoplast, another essential single copy organelle of secondary endosymbiotic origin, forms a comparable branched network, but divides prior to mitochondrial fission during blood- and liver-stage replication[9,11]. To produce viable offspring, the parasite has to ensure that each daughter parasite has a complete set of these organelles. However, so far a detailed view of these processes and the mechanisms involved is lacking.

We aimed to capture the process of mitochondrial division in detail using different imaging methods. However, this comes with several challenges. Firstly, imaging the small-sized parasites (1-7 μm diameter), and the even smaller organelles within the parasites, requires the use of super-resolution imaging techniques. Secondly, visualization of the mitochondrion requires a specific fluorescent marker or dye. Mitochondrial dyes, such as Rhodamine123 and MitoTracker™, have been widely used in the field[12]. These dyes rely on membrane potential to enter the mitochondrion and are therefore also used as a viability marker[13]. However, some of these dyes were tested in a drug screen and shown to be highly active against *P. falciparum* with IC50 values below 200 nM[14,15]. Additionally, in our hands MitoTracker signal can be diffuse, and therefore limit the resolution that is needed for the visualization of mitochondrial fission. Hence, we aimed to develop a reporter parasite line which harbors a fluorescent mitochondrial marker that allows imaging of this organelle in live and fixed conditions in all life-cycle stages of *P. falciparum*. To do this, we deployed a

similar strategy that has been used successfully in the rodent model *Plasmodium berghei*[16,17]. The targeting signal of the known mitochondrial protein HSP70-3 was fused with a fluorescent protein and integrated in a silent intergenic locus (SIL)[18]. Expression of this mitochondrial-localized fluorescent protein allowed visualization of the organelle during imaging of asexual, sexual and mosquito stages. Using high resolution confocal microscopy, we were able to make a detailed 3D map of different mitochondrial fission stages during schizogony in asexual blood stages. Focused ion beam scanning electron microscopy (FIB-SEM) image stacks from Evers *et al.* were used to confirm these mitochondrial fission stages with high detail[19]. This also allowed us to study apicoplast division and highlighted the potential role of the centriolar plaques (CPs) in apicoplast segregation. These different microscopic approaches empowered us to put forward a detailed model for mitochondrial and apicoplast division and distribution during the final stages of schizogony.

Results

To acquire a detailed understanding of mitochondrial fission and distribution, we set out to capture this process throughout the *Plasmodium* life cycle by combining different microscopy approaches. We stained mature blood-stage wild-type *P. falciparum* NF54 strain parasites with two different MitoTracker dyes and used these to visualize the mitochondrion in fixed confocal imaging. Surprisingly, both MitoTracker dyes showed a discontinuous, punctuated staining pattern (Figure 1A). FIB-SEM studies have confirmed the prevailing notion that the mitochondrion is a single, branched network during these schizont stages[19]. While this observation may arise from crosslinking of the MitoTracker dyes to specific proteins and aggregations thereof resulting from the fixation process, we concluded that the punctuated staining pattern is likely an artifact and consequently limits our ability to dissect and visualize the process mitochondrial fission. To address this, we developed a new fluorescent mitochondrial marker that can be used for imaging live and fixed samples (Figure S1).

Design and generation of a new mitochondrial marker parasite line

We designed a mitochondrial marker that consists of the promotor and mitochondrial targeting sequence of the gene encoding the mitochondrial heat shock protein 70 (HSP70-3, PF3D7_1134000), fused to an mScarlet red fluorescent protein (Figure S1A). HSP70-3 was selected based on its high and consistent expression profile throughout the whole life cycle and has been successfully used for the same purpose in *P. berghei*[16,17]. We aimed to stably integrate this fluorescent marker in the *P. falciparum* genome, without affecting any normal biological processes and parasite growth throughout the parasite life cycle. Selection of the new integration site, SIL7, is described extensively in Supplemental Information S1. The integration plasmid was transfected into NF54 parasites together with two different Cas9 guide plasmids directed at the SIL7 site. Successful integration of the mitochondrial marker and absence of WT parasite contaminations were confirmed by integration PCR (Figure S1B). A growth assay showed no difference in growth of the mitochondrial reporter line, MitoRed, compared to WT parasites in asexual blood stages (Figure S1C).

Characterization of the MitoRed parasite line

To visualize the mitochondrial marker, asexual blood-stage MitoRed parasites were fixed and used for fluorescent imaging. The fluorescent signal was well preserved after fixation and no antibody staining was required for mitochondrial visualization in all asexual blood stages (Figure 1B). To assess whether the punctuated mitochondrial morphology observed after MitoTracker staining was an imaging artifact or a morphological aberration caused by the dye, we stained MitoRed parasites with three different MitoTracker dyes. Discontinuous, punctuated mitochondria were observed in all MitoRed parasites stained with MitoTracker, while this was not observed in unstained MitoRed parasites (Figure 1C). The effect was less pronounced during live imaging of MitoTracker stained parasites (Figure S2). While there is an obvious imaging artifact following fixation of MitoTracker-stained blood-stage *P. falciparum* parasites, the altered MitoRed signal in the presence of the dye might even suggest possible changes in mitochondrial morphology.

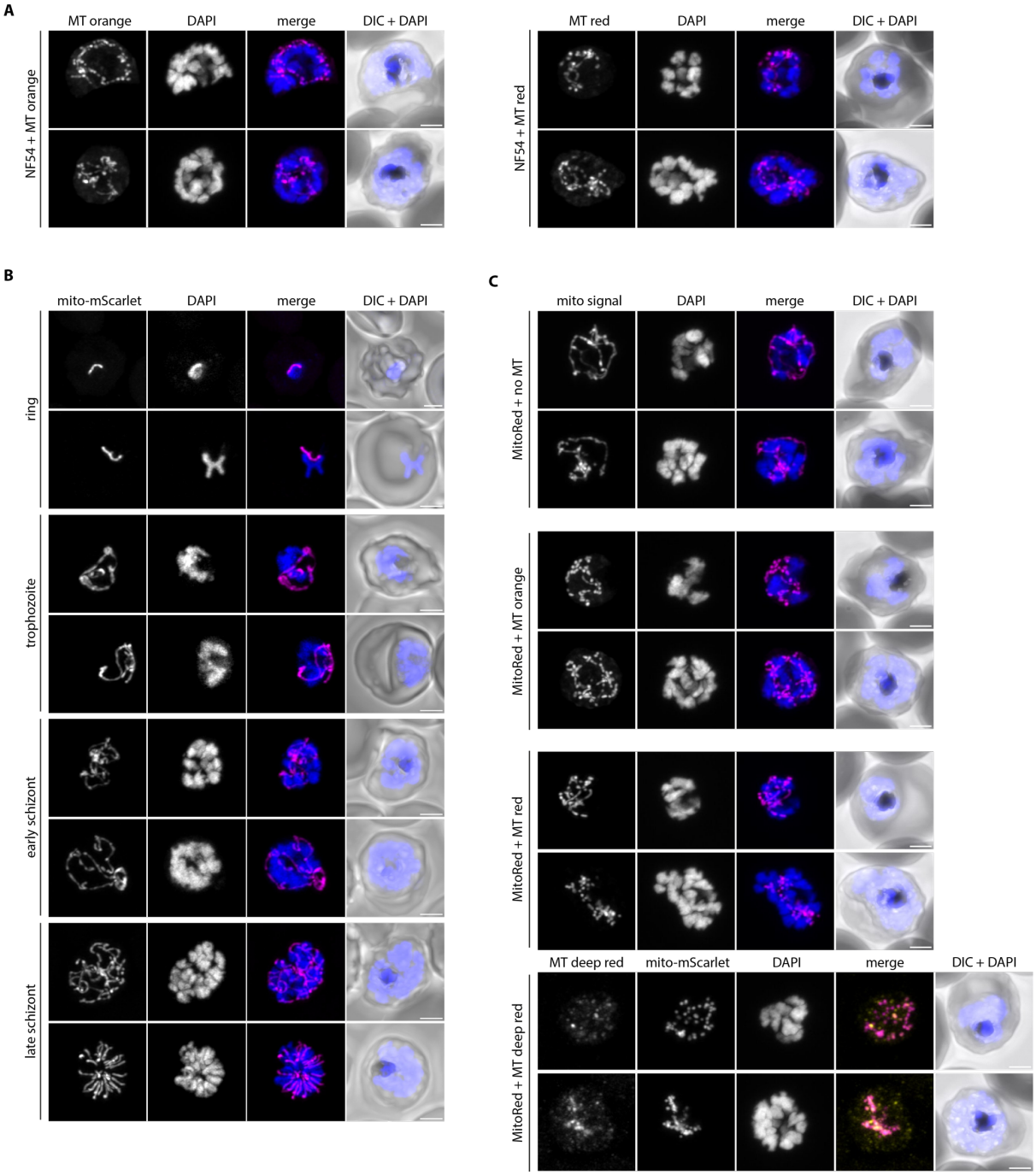

Figure 1. Comparison of MitoTracker and a new mitochondrial marker for fluorescence imaging. *A) Fluorescent imaging of WT parasites stained with MitoTracker Orange CMTMRos (MT orange) or MitoTracker Red CMXRos (MT red). B) Fluorescence microscopy of MitoRed. The mito-mScarlet signal was observed in all asexual life-cycle stages including rings, trophozoites, early and late schizonts. No antibody staining was used and fluorescent signal observed is exclusively the mito-mScarlet signal. C) Fluorescence microscopy of MitoRed, either unstained (no MT) or stained with MT orange, MT red or MitoTracker Deep Red FM (MT deep red). Mito signal is the combined MitoTracker and mito-mScarlet signal that is observed in this channel. All images are maximum intensity projections of Z-stacks taken with Airyscan confocal microscope. Scale bars, 2 μm.*

155 **Mitochondrial dynamics during gametocyte development and activation**
156 To study mitochondrial dynamics throughout the malaria parasite life cycle, MitoRed
157 parasites were induced to form gametocytes, which were fixed for microscopy on day 5, 7,
158 10, and 13 post induction. Parasites were stained for α tubulin to distinguish male and
159 female gametocytes in stage IV and V. In stage II and III gametocytes, the mitochondrion
160 appears as a small knot that increases slightly in size when gametocytes become more
161 mature (Figure 2A). This is consistent with our FIB-SEM data[19]. Evers *et al*. also showed that
162 gametocytes have multiple mitochondria already from early gametocyte development
163 onwards. Although light microscopy does not provide the resolution or ability to show
164 membrane boundaries to distinguish the multiple mitochondria in stage II and III
165 gametocytes, in stage IV gametocytes we could clearly observe separate mitochondria in
166 both male and female gametocytes (Figure 2A, Figure S3A). There is no clear difference in
167 stage IV gametocytes between male and female mitochondria. However, in stage V
168 gametocytes the mitochondria in males appear slightly more dispersed, while the female
169 mitochondria remain compact (Figure 2A, Figure S3B). Data from Evers *et al.* support this
170 and showed consistently smaller volume and more loosely packed mitochondria in males
171 compared to females[19]. When gametocytes are taken up by the mosquito via a blood meal,
172 they are activated and transform into extracellular male and female gametes. While the
173 female gametocyte develops into a single macrogamete, male gametocytes form up to eight
174 flagellated microgametes. This transformation is triggered by a temperature drop and
175 xanthurenic acid present in the mosquito midgut[20]. Upon *in vitro* activation, the difference
176 between male and female mitochondria becomes more evident. Mitochondria in females
177 remain in a compact knot while the parasite rounds up (Figure 2B). Interestingly, in males
178 the mitochondria become smaller and more dispersed, and sometimes round up to small
179 bean-like structures (Figure 2B, Figure 2D). This process already starts 2 minutes after
180 activation. While this particular activation experiment was performed on a gametocyte
181 culture that did not exflagellate for unclear reasons, it was repeated several times and very
182 similar results were found in exflagellating males (Figure 2C). An association of mitochondria
183 with flagella is not uncommon and can also be observed in *e.g.* kinetoplastids, such as
184 *Trypanosoma* and *Leishmania spp*, where the mitochondrion resides at the base of the
185 flagellum, and in human sperm cells, where the mitochondrion wraps around the base of
186 the flagellum to provide energy for flagellar movement[21]. In some exflagellating males, we
187 found close apposition of the dispersed mitochondrion to the axonemes (Figure S4),
188 although this was not consistent.
189
190 **Mitochondrial dynamics in mosquito stages**
191 In the mosquito midgut, the male microgamete seeks out a female gamete for fertilization.
192 After fertilization, the zygote takes one day to transform into a motile ookinete, which can
193 traverse the midgut epithelium and differentiate into an oocyst. This oocyst expands and
194 motile sporozoites are formed within the oocyst. When fully matured, the oocyst will burst
195 and sporozoites will egress, spread through the hemolymph system, and invade the
196 mosquito salivary glands. During oocyst development, the parasite mitochondrion has to
197 expand enormously and then be divided over thousands of daughter sporozoites. However,
198 very little is known about mitochondrial dynamics and only few studies have visualized the
199 mitochondrion during these stages[16,22,23].
200

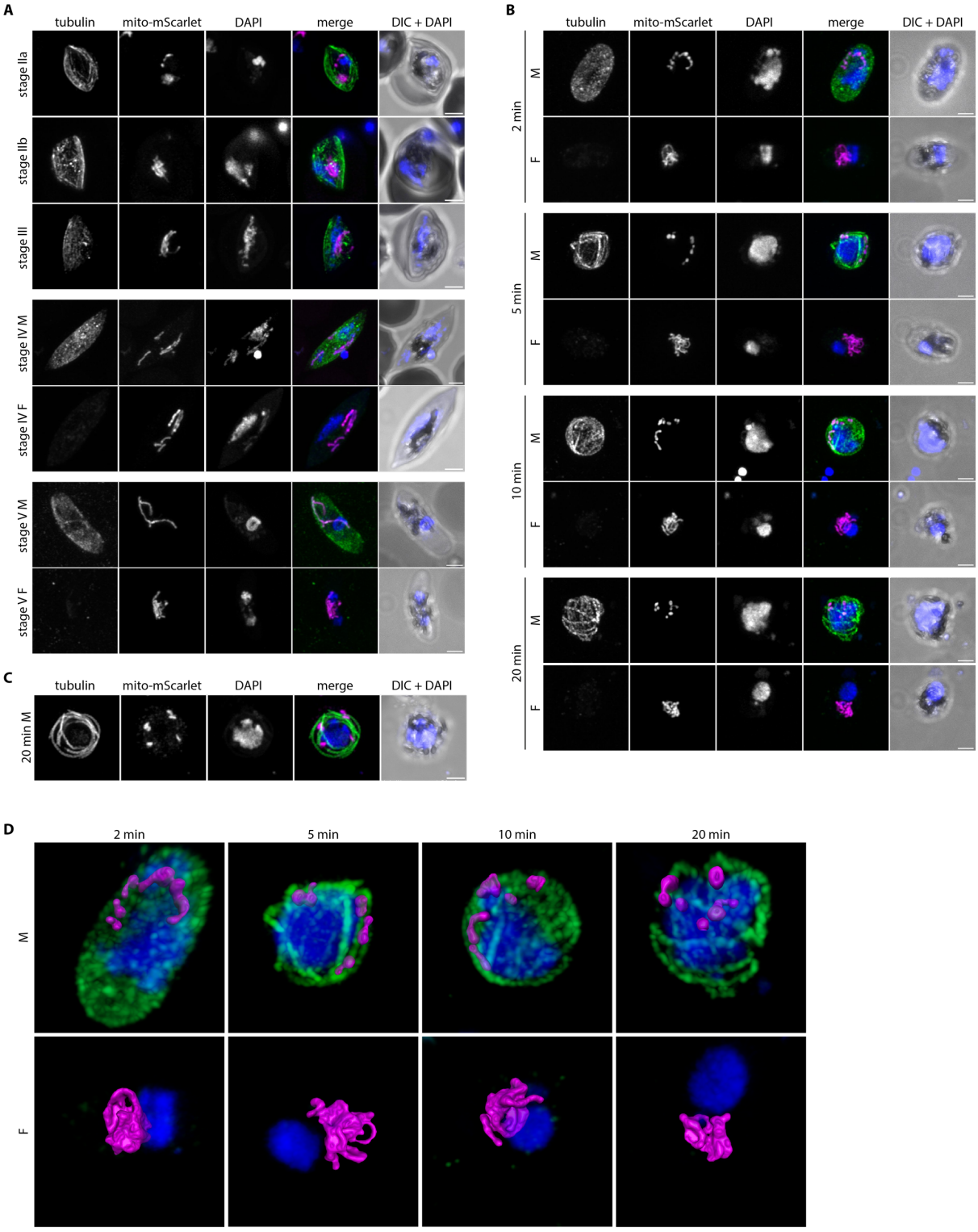

201
202
203 ***Figure 2. Mitochondrial dynamics during gametocyte development and activation.*** *A)*
204 *Immunofluorescence assay on MitoRed gametocytes stages IIa, IIb, III, IV, and V, stained with anti-β-*
205 *tubulin (green) and DAPI (DNA, blue). The mito-mScarlet signal is shown in magenta. In stage IV and V,*
206 *male (M) and female (F) gametocytes are distinguished based on the intensity of the tubulin signal (males*
207 *high, females low). B) Immunofluorescence assay on MitoRed parasites during different stages of*
208 *gametocyte activation (2, 5, 10 and 20 minutes after activation). C) Immunofluorescence assay on*
209 *MitoRed exflagellating male gamete 20 minutes after activation. A-C) Images are maximum intensity*
210 *projections of Z-stacks taken with an Airyscan confocal microscope. Scale bars, 2 μm. D) 3D visualization*

211 *of male and female MitoRed parasites 2, 5, 10, and 20 minutes after activation. The mito-mScarlet*
212 *fluorescent signal is segmented based on manual thresholding.*
213
214 To explore if MitoRed parasites develop normally in the mosquito and to visualize
215 mitochondrial morphology, mature MitoRed gametocytes were fed to *Anopheles stephensi*
216 mosquitoes. One day after the feed, the mosquito blood bolus was extracted and stained
217 with anti-*Pf*s25 conjugated antibodies to visualize ookinetes by live microscopy. We
218 distinguished different stages of ookinete maturation as described by Siciliano *et al.*[24]. Due
219 to the resolution limit of light microscopy, it was difficult to tell if there were one or multiple
220 mitochondria as observed in gametocyte stages. Since we did not find evidence for the
221 presence of multiple mitochondria in these ookinete development stages, we will refer to it
222 as "the mitochondrion" in the coming paragraph, although we cannot rule out the presence
223 of multiple mitochondria. During earlier stages of ookinete development (II), when
224 ookinetes have a short protuberance attached to the round body, the mitochondrion
225 resides in the round body (Figure 3A, 3B). When the protuberance starts to elongate
226 further, one elongated mitochondrial branch stretches out and reaches into the
227 protuberance. In stage III ookinetes, the mitochondrion stretches out further into the
228 growing protuberance, spiraling out from the round body. We could not find clear stage IV
229 ookinetes where the protuberance is at its full length, which could be explained by the swift
230 development from stage IV to V ookinetes as was observed by Siciliano *et al.*[24]. However, in
231 the mature stage V ookinetes, the mitochondrion appears as a tight knot in the main
232 parasite body.
233
234 At day 7, 10, and 13 after infection, mosquitoes from a feed with an infection rate of 100%
235 and an average of 5 oocysts/mosquito were dissected and midguts were used for live
236 confocal microscopy. At day 7, small oocysts were observed with a branched mitochondrial
237 network stretched out throughout the cell (Figure 3C). Segmentation of the fluorescent
238 signal based on manual thresholding indicated that the mitochondrion consisted of one
239 fragment. Day 10 oocysts were much larger and the mitochondrial mesh-like network
240 appeared more organized, also localizing to areas directly below the oocyst wall (Figure 3D).
241 At day 13, oocysts of various sizes were observed. Some large oocysts showed a highly
242 organized mitochondrial network, where mitochondrial branches were organized in a radial
243 fashion around a central organizational point (Figure 3E, S5A). We named these points
244 mitochondrial organization centers (MOCs). At least tens of these MOCs could be observed
245 per cell. Some small oocysts at day 13 showed structures that looked like beginning MOCs
246 (Figure S5B). However, several small oocysts showed a dispersed, globular mitochondrial
247 signal, which we interpreted as unhealthy or dying parasite (Figure S5C). While several free
248 sporozoites were observed in dissected midguts and salivary glands on day 16 (data not
249 shown), we never observed an oocyst containing fully mature sporozoites with a divided
250 mitochondrion or an infected salivary gland on day 16 and 21 after infection. This indicates
251 that either the mitochondrial marker itself, or integration in the SIL7 locus causes issues for
252 sporozoite development. We conclude that the MitoRed line is a great tool for
253 mitochondrial visualization in asexual blood stages, gametocytes stages, and mosquito
254 stages up until late oocysts (Supplemental Information S1).
255

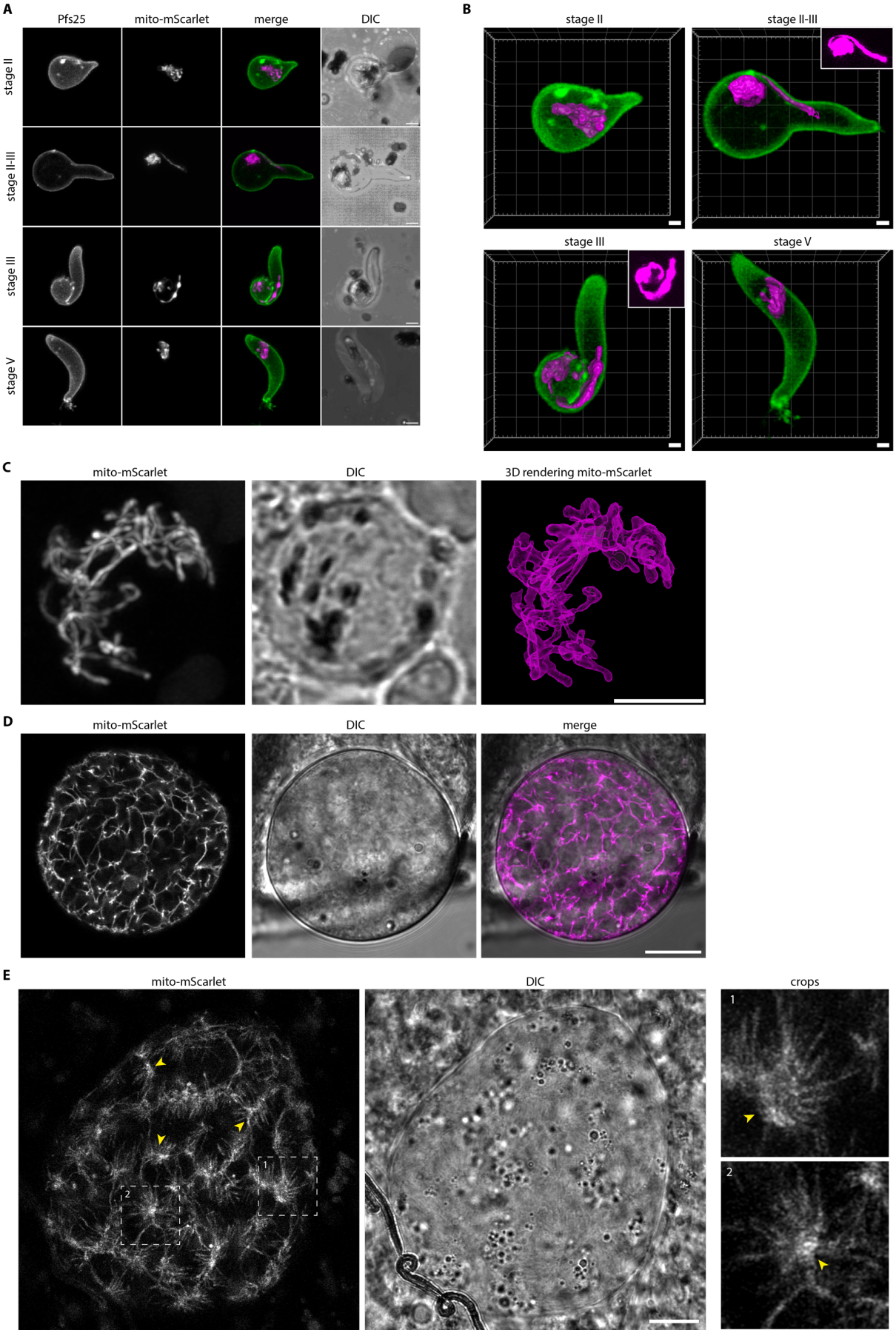
A
Pfs25
mito-mScarlet
merge
DIC
stage II
stage II-III
stage III
stage V
B
stage II
stage II-III
stage III
stage V
C
mito-mScarlet
DIC
3D rendering mito-mScarlet
D
mito-mScarlet
DIC
merge
E
mito-mScarlet
DIC
crops
1
2

256
257

258 ***Figure 3. Mitochondrial dynamics during mosquito stage development.*** *A) Live imaging of MitoRed*
259 *ookinetes one day after mosquito feed. Different stages of ookinete maturation (II – IV) were*
260 *distinguished based on description by Siciliano* et al.[24]*. Cells were stained with an Alexa fluor 488*
261 *conjugated anti-Pfs25 antibody to visualize parasite outline (green). Images are maximum intensity*
262 *projections of Z-stacks taken with an Airyscan confocal microscope. Scale bars, 2 μm. B) 3D visualization*
263 *of different ookinete maturation stages. The mito-mScarlet fluorescent signal is segmented based on*
264 *manual thresholding. Two smaller images in upper right corner of stage II-III and stage III are crops of the*
265 *mitochondrial fluorescent signal with increased brightness and contrast. Scale bars, 1 μm. Live imaging of*
266 *MitoRed oocysts on day 7 (C) day 10 (D) and day 13 (E) after mosquito infection. C) Oocyst at day 7 after*
267 *infection with left image showing a maximum intensity projection of the mito-mScarlet signal. Right*
268 *image shows a segmentation of the mito-mScarlet fluorescent signal by thresholding in Arivis software.*
269 *Scale bar, 4 μm. E) oocyst at day 13 after infection. Images on the right are crops of the mito-mScarlet*
270 *signal of the image on the left, indicated by the dotted-line areas. Yellow arrowheads indicate*
271 *mitochondrial organization centers (MOCs). D-E) Scale bars, 10 μm.*
272
273 **Mitochondrial division during schizogony in asexual blood stages**
274 Next, we aimed to use MitoRed for live visualization of mitochondrial division during
275 schizogony in asexual blood stages. The biggest advantage of live imaging is that one
276 parasite can be followed over time to capture mitochondrial fission events chronologically.
277 Unfortunately, this proved to be challenging. All parasites imaged in several experiments for
278 a duration exceeding 60 minutes exhibited significant morphological alterations, including
279 mitochondrial swelling, fragmentation, and formation of vesicle-like structures, which
280 indicate an unhealthy or dying parasite (Figure S6A). Additionally, we frequently observed
281 parasites egressing from their RBCs after approximately 45 minutes of imaging, indicating
282 that imaged parasites are unhealthy (Figure S6B). Optimizing imaging conditions by reducing
283 laser power, increasing time interval, better temperature control, and gassing of the
284 imaging chamber with low oxygen mixed gas (3% O_2, 4% CO_2), did not improve parasite
285 health during imaging. Therefore, we decided to go for a fixed imaging approach to capture
286 mitochondrial division in asexual blood-stages.
287
288 To capture mitochondrial fission, MitoRed parasites were tightly synchronized and fixed
289 between 32-36 and 36-40 hours after invasion. In our culture system, MitoRed parasites
290 have a replication cycle of approximately 40 hours, so we captured the last eight hours of
291 schizont maturation before merozoite egress from the RBC. In order to distinguish the
292 precise stage of schizont maturation, we included an anti-GAP45 antibody staining.
293 Glideosome associated protein 45 (GAP45) is an inner membrane complex (IMC) protein
294 and is important for RBC invasion[25,26]. IMC formation starts at the apical end of a developing
295 merozoite during schizogony and continues to develop until it fully encapsulates the
296 daughter merozoite with its own IMC membrane[27,28]. We used the stage of IMC formation
297 and therefore merozoite segmentation as a marker for the maturity and age of the
298 schizonts. Based on IMC and DNA staining, we differentiated four stages of schizont
299 maturation: pre-segmentation (n=6), early-segmentation (n=9), mid-segmentation (n=15),
300 and late-segmentation (n=10, Figure 4).
301
302 We generated and classified Z-stack images of 40 schizonts, which allowed us to reconstruct
303 a timeline of mitochondrial fission. During pre- and early-segmentation stages, the branched
304 mitochondrial network stretches throughout the parasite. Only at the end of early-
305 segmentation stages, when the IMC is approximately halfway formed, the mitochondrion is
306 oriented around the food vacuole in the center of the parasite with its branches pointing

307 outwards in a radial fashion, creating a "cartwheel"-like structure (Figure 4). As the IMC
308 progresses further and schizonts enter the mid-segmentation stage, this mitochondrial
309 cartwheel structure is divided into smaller fragments, which maintain their radial branch
310 orientation into the segmenting merozoites. Only when IMC formation appears complete,
311 did we observe mitochondria that are entirely divided and distributed over the daughter
312 merozoites. This highlights the extremely late timing of this process.
313

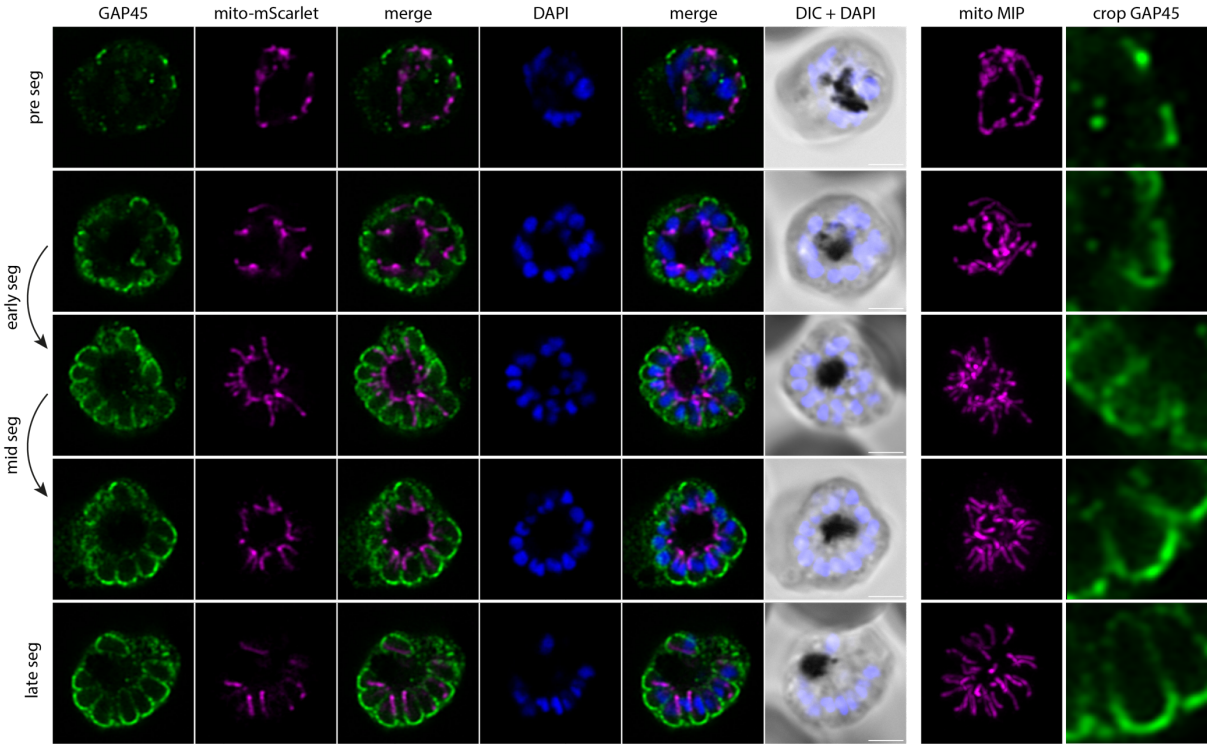

314
315
316 ***Figure 4. Mitochondrial fission in asexual blood-stage parasites.*** *Immunofluorescence assay on MitoRed*
317 *schizonts stained with anti-GAP45 antibody (green) to visualize IMC and DAPI (DNA, blue). The mito-*
318 *mScarlet signal is shown in magenta. Four different stages of schizont maturity are distinguished: pre-*
319 *segmentation (pre seg), schizonts still undergo nuclear division (nuclei are large and irregularly shaped)*
320 *and there is no, or very little IMC staining without clear curvature. Early-segmentation (early seg),*
321 *schizonts have (almost completely) finished nuclear division (nuclei are small and round), there is a clear*
322 *IMC signal that has a curved shape at the apical end of the forming merozoites but is less than half-way*
323 *formed. Mid-segmentation (mid seg), the IMC of the segmenting merozoites in these schizonts is more*
324 *than half-way formed, but there is still a clear opening at the basal end of the merozoite. Late-*
325 *segmentation (late seg), in these schizonts the IMC seems to be completely formed with no clear opening*
326 *at the basal end of the forming merozoites. Images are single slices of a Z-stack taken with an Airyscan*
327 *confocal microscope. Images of the mito-mScarlet signal in the seventh column are maximum intensity*
328 *projections (MIPs). Images in the eighth column are zoom-ins of the GAP45 signal depicted in the first*
329 *column. Scale bars, 2 μm.*
330
331 To further quantify the numbers and sizes of mitochondria and to create 3D renderings of
332 the mitochondrial network throughout segmentation, we utilized threshold-based masking
333 of the fluorescent signal (Figure 5). During pre- and early-segmentation stages, the
334 mitochondrial network consists of one large fragment (between 7-14 μm^3), often with 1-3
335 smaller fragments (<1.5 μm^3) (Figure 5AI, 5AII). As evident from our FIB-SEM data (Figure
336 S9A), the mitochondrion features constricted regions, characterized by notably reduced
337 diameters. Hence, the smaller fragments observed during these stages are likely not

338 autonomous but caused by the reduced fluorescent marker intensity in the constricted
339 regions. At the end of early-segmentation stages when the IMC is almost halfway formed,
340 the mitochondrial network starts to orient itself in a radial fashion around the center of the
341 parasite (Figure 5AII), consistent with the 2D image analysis (Figure 4). During mid-
342 segmentation stages, the radial mitochondrial branches elongate further into the
343 developing merozoites, and the large mitochondrial fragment is divided in smaller
344 fragments at the center of the cartwheel structure (Figure 5AIII). There is a slight increase in
345 number of mitochondrial fragments per parasite, specifically the "intermediate" sized
346 mitochondrial fragments of 1-4 μm^3. Only in the last stage of merozoite segmentation, there
347 is a big increase in the number of mitochondrial fragments (Figure 5C). Of note, there
348 appears to be no correlation between this number and the number of nuclei in the parasites
349 (Figure 5B, 5C). A likely technical explanation is the limited Z-resolution of light microscopy
350 and the different nuclear and mitochondrial segmentation methods. When mitochondrial
351 fragments are located closely above each other, the limited Z-resolution in combination
352 with threshold-based masking can cause the adjacent fragments to appear as one
353 continuous structure. Therefore, the number of mitochondrial fragments per schizonts will
354 be underestimated in these late schizont stages. The nuclei on the other hand were
355 segmented through an automated (spherical) object detection algorithm which does not
356 have this problem. Even when the IMC formation appears to be completed based on the
357 GAP45 staining, only 20% of cells appear to have concluded mitochondrial fission as
358 indicated by exclusively containing homogenously small sized mitochondrial fragments (<1.0
359 μm^3) (Figure 5AIV). During the late segmentation stage, some parasites still have a large
360 mitochondrial fragment of more than 5 μm^3, while others only have small and intermediate
361 sized mitochondrial fragments (Figure 5D). This suggest that division of the mitochondrial
362 cartwheel structure into small fragments is a fast, stepwise process that does not happen in
363 a 2^n progression and happens only in the final moments of merozoite segmentation.
364

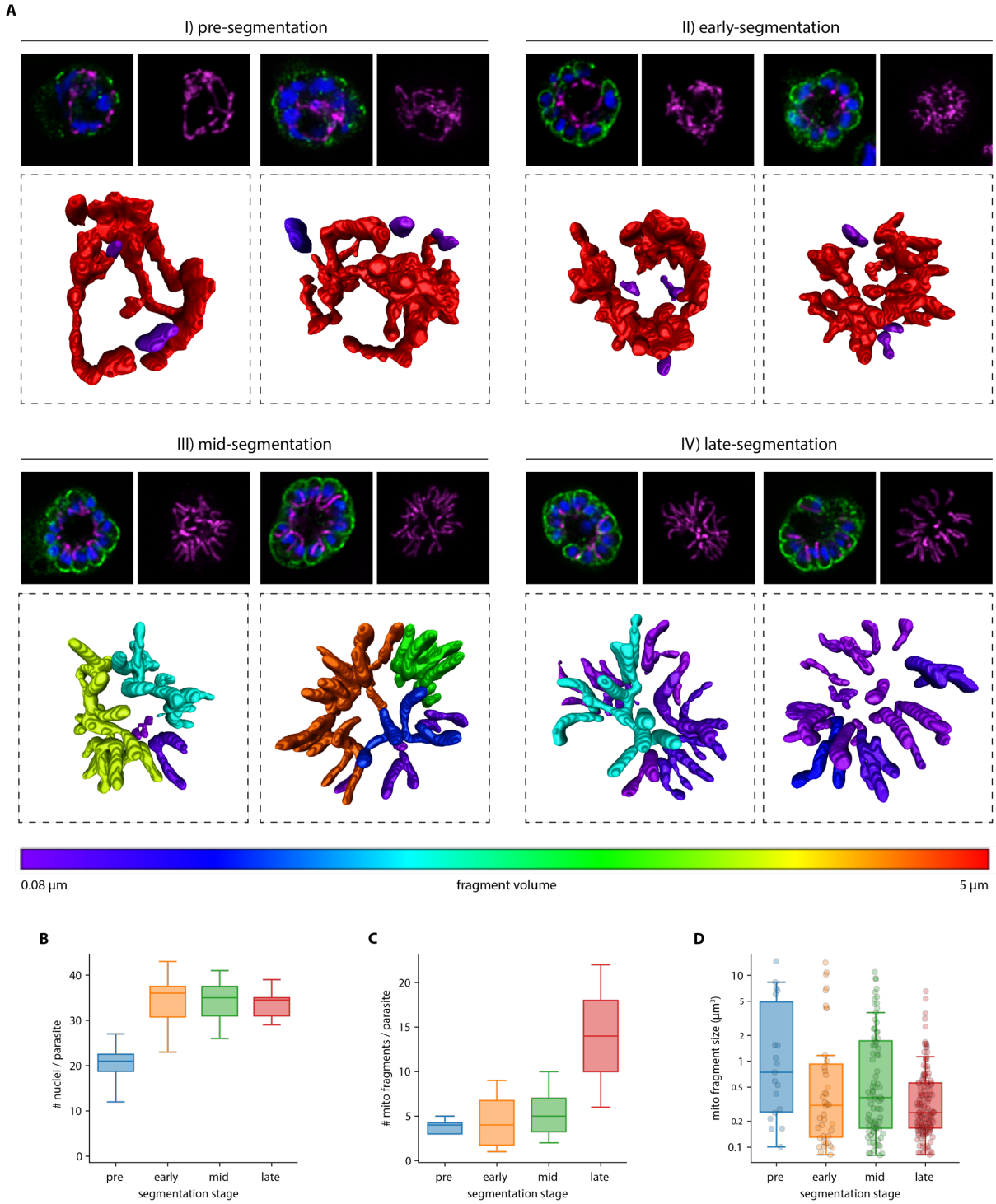

Figure 5. 3D analysis of mitochondrial fission stages during schizogony. *A) 3D visualization of mitochondrial segmentations based on thresholding of the mito-mScarlet signal in Arivis image analysis software. Smaller images in top row are a single slice of the Z-stack with anti-GAP45 labelling (IMC, green), DAPI (DNA, blue) and mito-mScarlet (magenta), and a maximum intensity projection of the mito-mScarlet signal. The larger bottom picture is a 3D visualization of the segmented mitochondrial signal. The color of the mitochondrial fragment represents the size of this fragment, as is shown in the color bar at the bottom. Two representative parasites are depicted for each of the four segmentation stages defined in Figure 4. B) Boxplot indicating the number of nuclei per parasite in the different segmentation stages. C) Boxplot indicating the number of mitochondrial fragments per parasite in the different*

segmentation stages. D) Boxplot indicating the size of the mitochondrial fragments in the different segmentation stages.

Visualization of mitochondrial and apicoplast division using volume electron microscopy

Although the use of light microscopy allowed us to reconstruct mitochondrial fission in good temporal resolution, its limited spatial resolution and reliance on indirect staining leaves some questions unanswered. Our recent volume electron microscopy study detailed parasite organelle structures at a nanometer resolution bringing many new insights to the light[19]. Here, we reused the underlying FIB-SEM data, which besides gametocytes also contains asexual blood-stage parasites from different stages, to examine mitochondrial fission with high resolution. Asexual parasites in different stages of schizogony were selected and organelles including nuclei, mitochondrion, and apicoplast were segmented for 3D rendering (detailed description per parasite in Tables S2 and S3). In line with the results from our light microscopy experiments, the mitochondrion is a large, branched network stretched throughout the cell in early schizont stages before segmentation has started (Figure 6, Movie 1). The apicoplast is also a branched network, however, it is much smaller than the mitochondrion (Table S2). The apicoplast network is divided into smaller fragments of different sizes when nuclear division is still ongoing and IMC formation has started (Figure 7, Table S3, Movie 4). When nuclear division is finishing and the IMC envelops part of the nucleus, apicoplast division is completed (Figure 6, Movie 5). The mitochondrion starts to orient its branches in a radial fashion towards the developing merozoites. When nuclear division is completely finished and the IMC envelops most of the nucleus, the mitochondrion forms a clear cartwheel structure with its branches pointing into the developing merozoites (Movie 6). During late segmentation stages, where only a small opening is connecting the merozoite to the residual body, the mitochondrion is divided into smaller fragments of various sizes (Movie 7). While some mitochondrial fragments have a volume comparable with the mitochondria in a fully segmented parasite (0.016 - 0.036 μm^3), other fragments are still 2-4 times that volume (Figure S7).* These larger mitochondrial fragments have several branches that are pointing into developing merozoites but are still connected to each other outside the merozoites. In an almost fully segmented schizont, where most merozoites are fully developed and only few merozoites are still connected to the residual body through a small opening, the mitochondrial division is completed and the number of mitochondrial fragments is the same as the number of merozoites (Movie 8). These findings corroborate our light microscopy data and confirm the mitochondrial division stages, position of relevant structures not stained in light microscopy, and timing of mitochondrial and apicoplast division during schizogony.

** Note: The volumes measured in the FIB-SEM data differ greatly from the volumes measured in the 3D fluorescent microscopy data. This can be explained by the limited spatial resolution of fluorescent microscopy because of the diffraction of light. The diffraction limit of the confocal Airyscan microscope that was used is ~120 nm in lateral direction and ~350 nm in axial direction. The diameter of the mitochondrion in asexual blood-stage parasites is ~140 nm, which is at the edge of the resolution limit. Therefore, the volume measurements of thresholding-based segmentation of the fluorescent signal are not very accurate and quickly over-estimate the volume. These volume estimations should merely be used to compare relative volumes of mitochondrial fragments. The FIB-SEM data has a resolution of 5 nm in lateral direction and 15 nm in axial direction, which allows much more precise visualization of organelles and volume measurements.*

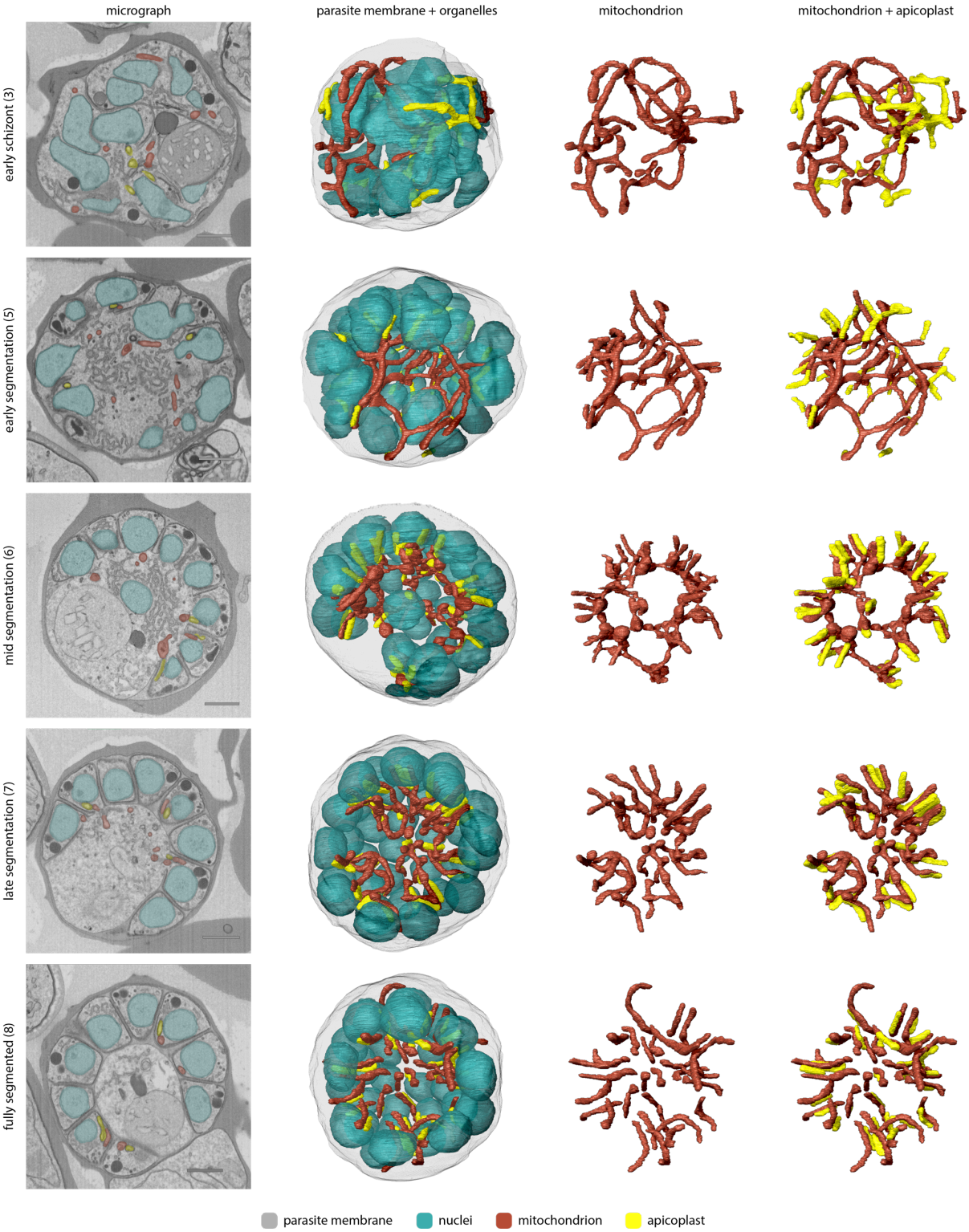

Figure 6. 3D rendering of mitochondrion and apicoplast during different stages of schizogony. *First column contains representative micrograph images from different schizont stages. The numbers between brackets indicate the parasite ID number and detailed information can be found in table S2 and S3. Scale bars, 1 μm. The second, third and fourth column contain 3D renderings of parasite membrane (gray, 5% transparency) nuclei (teal, 50% transparency), mitochondrion (red) and apicoplast (yellow).*

433 **Interaction between mitochondrion and apicoplast in late stage schizonts**
434 During schizogony, the mitochondrion and apicoplast show different moments of close
435 association. Prior to apicoplast division, the mitochondrion and apicoplast have several
436 apposition sites, which have also been described by Evers *et al.*[19] (Figure S8A and S8B). It
437 remains unclear if these close associations represent true membrane contact sites that
438 facilitate the exchange of metabolites or lipids between the organelles, or if these are
439 merely random due to the limited space in the parasite. When apicoplast division is finished,
440 the endings of the mitochondrial branches reach towards the basal endings of the
441 apicoplasts (Figure S8D). Subsequently, the branches of the mitochondrial cartwheel
442 structure align with the apicoplast over its entire length (Figure S8C and S8D). This close
443 alignment remains when mitochondrial division is complete.
444
445 **Bulbous mitochondrial structures with double membrane invaginations**
446 The parasite mitochondrion does not have a consistent diameter during schizogony. While
447 some parts have a very small diameter other areas of the mitochondrion are more bulbous
448 (Figure S9A). These bulbous parts often contain double membrane invaginations of various
449 size and shape (Figure S9C, S9D, S9F). These bulbous invagination structures (bulins) are
450 found in all schizont stages and vary greatly in shape, size, and location in the mitochondrial
451 network. In early stage schizonts, bulins can be found at branching points and in the middle
452 of a continues branch of the mitochondrial network (Figure S9D, S9F). However, during mid-
453 segmentation stages, when the mitochondrion is oriented in its typical cartwheel structure,
454 bulins are consistently observed at the base of a mitochondrial branch near the merozoite
455 entrance (Figure S9D, S9F). These merozoite-entrance bulins were found in all eight mid-
456 segmentation stage schizonts from two independent experiments (example shown in Movie
457 9). Bulbous areas at the base of mitochondrial branches are also observed with fluorescent
458 microscopy (Figure S9B). This, and the specific location of bulins, makes them unlikely an
459 artifact of fixation or sample preparation for the FIB-SEM, although this cannot be ruled out
460 completely. Bulins that reside at the entrance of a forming merozoite during the cartwheel
461 phase are typically characterized by contact with the basal end of the divided apicoplast,
462 and a small constriction right above the bulin where the mitochondrial branch enters the
463 merozoite (Movie 10). Bulbous areas at the base of the mitochondrial branches are also
464 observed with fluorescent microscopy (Figure S9B). In late-segmentation schizonts, we
465 observed small bulins at the base of a divided mitochondrial fragment or at the entrance of
466 a merozoite when the mitochondrial branch was not yet divided (Figure S9D, S9F).
467 Sporadically, we also found bulins in the apicoplast (Figure S9E). The significance and
468 function of these bulins remain to be explored, but it is tempting to speculate about a
469 possible role in organelle division.
470
471 **Centriolar plaques associate with apicoplast but not mitochondrion during organelle**
472 **segregation**
473 In mammalian cells, segregation of organelles is coordinated by microtubules that arise
474 from the centrosomes, or so-called microtubule organizational centers (MTOCs).
475 *Plasmodium* parasites lack canonical centrosomes but organize their mitotic spindle from a
476 structure called the centriolar plaque (CP), which is embedded in the nuclear envelope[29,30].
477 Expansion microscopy studies from Liffner *et al.* have suggested an association of the CPs
478 with both the mitochondrion and the apicoplast during schizogony, suggesting their
479 involvement in organelle segregation[31]. In our FIB-SEM images, we can distinguish the CP by

480 electron dense coffee filter-shaped regions in the nucleus (Figure 7A). In an early schizont
481 that still lacks IMC or rhoptries, nuclei contain one or two CPs, which are oriented to the
482 periphery of the parasite. 3D renderings show no direct association between the CPs and
483 the mitochondrion or apicoplast (Figure 7B, Movie 1). The distances between the
484 mitochondrion and CPs seems to be significantly smaller than the apicoplast-CPs distances.
485 This can be explained by the fact that the apicoplast is located in the center of the parasite,
486 while the mitochondrion is larger and stretched throughout the whole cell leading to
487 coincidental proximity to the peripheral CPs. In slightly later stage schizonts where IMC and
488 rhoptry formation has started, all nuclei contain either two CPs, or one CP that is dividing. A
489 portion of the CPs associated with the apicoplast, specifically with the endings of apicoplast
490 branches (Movie 2). When the IMC is developed slightly further, all CPs associate with the
491 apicoplast over the total length of the peripherally localized apicoplast network (Movie 3).
492 Usually, two CPs from the same nucleus associate with one apicoplast branch (Figure S10A).
493 However, sometimes two CPs from the same nucleus associate with completely different
494 branches of the apicoplast network (Figure S10B). There does not seem to be a specific
495 association between the mitochondrion and the CPs, and distances between the CPs and
496 apicoplast are significantly smaller compared to the CP-mitochondrion distances (Figure 7B).
497 The association between CPs and apicoplast continues during and after apicoplast division
498 (Movie 4-7). After apicoplast division, each apicoplast fragment is associated with one CP at
499 its peripheral end (Movie 5). During mid-segmentation stages, the endings of the
500 mitochondrial branches are close to the CPs (Movie 6). However, this seems to be a result of
501 the close association of the mitochondrion with the apicoplast, rather than a direct
502 interaction between the mitochondrion and the CPs. In a fully segmented schizont, the CPs
503 were much smaller and did not show a clear extranuclear compartment (Movie 8). This
504 close and very consistent association between the apicoplast and the CP, suggest an
505 important role in apicoplast segregation, while the mitochondrion likely deploys different
506 mechanisms to accomplish its proper distribution over the forming merozoites.
507
508
509

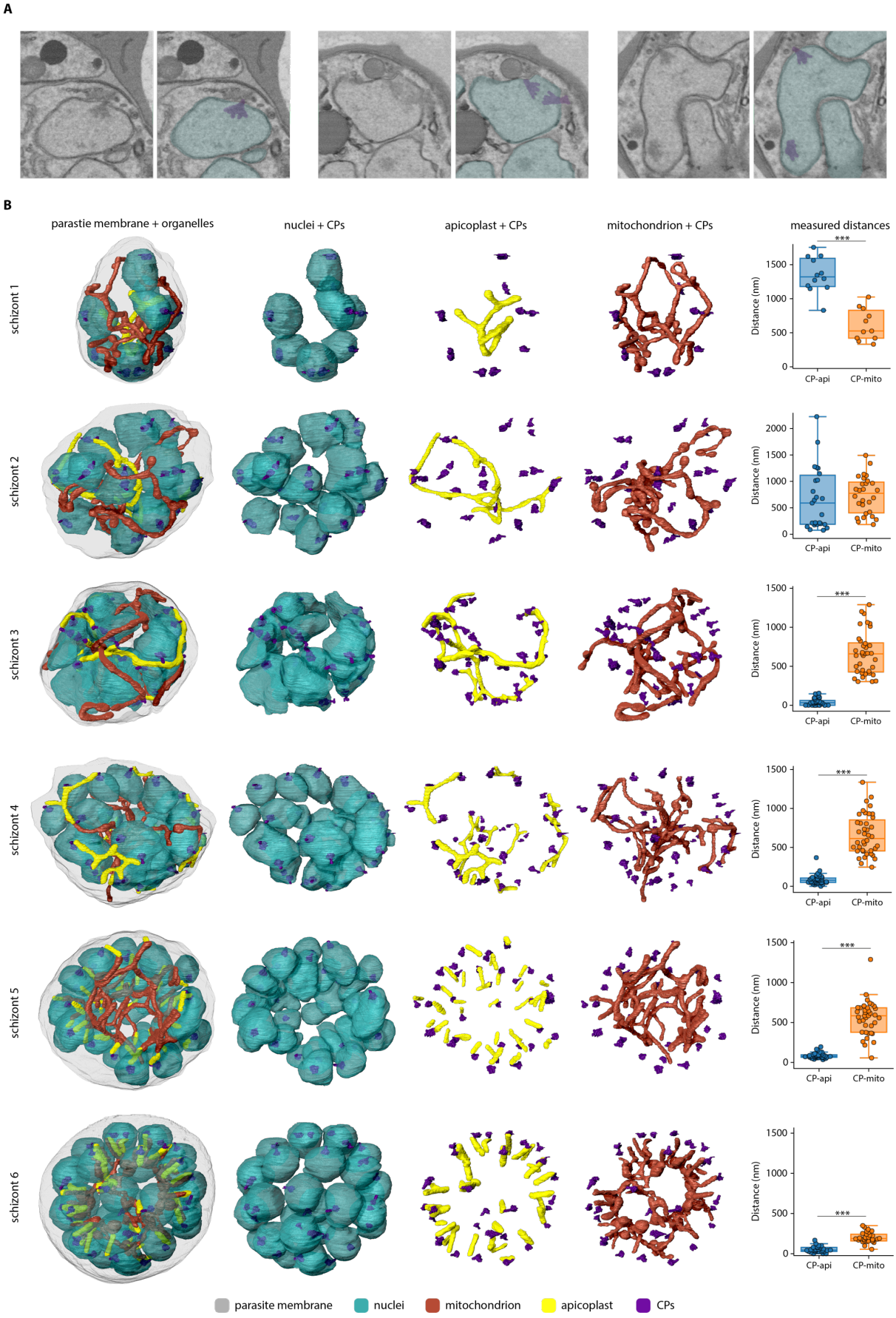
A
B
parastie membrane + organelles
nuclei + CPs
apicoplast + CPs
mitochondrion + CPs
measured distances
schizont 1
schizont 2
schizont 3
schizont 4
schizont 5
schizont 6
Distance (nm)
CP-api
CP-mito
***
parasite membrane
nuclei
mitochondrion
apicoplast
CPs

512 ***Figure 7. Association of apicoplast and not the mitochondrion with centriolar plaques during schizont***
513 ***development.*** *A) Micrograph images of nuclei (teal) with centriolar plaques (CPs, purple). B) 3D rendering*
514 *of nuclei (teal), apicoplast (yellow), mitochondrion (red), CPs (purple) and parasite membrane (gray, 5%*
515 *opacity). Parasite ID numbers are indicated on the left side of the micrograph images. Right column shows*
516 *measured distances between CPs and closest point to the apicoplast or mitochondrion. *** indicates $p <$*
517 *0.001.*
518
519
520
521

522 ## Discussion

523 In contrast with most eukaryotes, the fast-replicating *P. falciparum* asexual blood-stage
524 parasites harbor only a single mitochondrion. Consequently, proper division and distribution
525 of this organelle during schizogony is crucial to ensure all daughter cells receive a
526 mitochondrion. Here, we visualized the poorly understood mitochondrial dynamics in blood-
527 and mosquito-stages using a new parasite line with a fluorescent mitochondrial marker and
528 super-resolution 3D imaging methods. During blood-stage schizogony, a cartwheel structure
529 is formed and divided into smaller, unequally sized mitochondrial fragments in a stepwise
530 process. Final division into single mitochondria happens during the last stage of merozoite
531 segmentation. These division steps were cross validated by analyzing available FIB-SEM data
532 with nanometer resolution. This also allowed us to reconstruct apicoplast division and its
533 interactions with the mitochondrion. Finally, we showed that the apicoplast but not the
534 mitochondrion associates with the CPs during merozoite formation.
535
536 To date, the visualization of *Plasmodium* mitochondria has largely relied on MitoTracker
537 dyes. However, these dyes are toxic at nanomolar concentrations[14,15] and our data suggest
538 that they may alter mitochondrial morphology (Figure 1). We developed a reporter parasite
539 line harboring a fluorescent mitochondrial marker that shows a more continuous and less
540 punctuated staining pattern compared to MitoTracker dyes and is compatible with live and
541 fixed imaging without necessitating antibody labeling. Unfortunately, MitoRed is not well
542 suited for long-term time lapse imaging (>1h) since parasites showed various signs of poor
543 health, probably due to phototoxicity. While expansion microscopy is currently not feasible
544 with MitoRed, addition of a linear epitope tag would make this marker compatible with the
545 required denaturation step.
546
547 In line with our earlier observations, we demonstrated multiple mitochondria in gametocyte
548 stages[19]. As discussed by Evers *et al.*, there are several possible reasons for the emergence
549 of multiple mitochondria in gametocytes, such as adaptation to a metabolically varied
550 environment, distribution mechanism of mtDNA, or management of reactive oxygen
551 species. We expand upon these observations by also imaging gametocytes during activation.
552 In males, mitochondria become more dispersed while female mitochondria remain in a tight
553 knot. One possible explanation for this is that mitochondria in males are distributed to
554 specific locations in the cell to provide energy locally for certain processes. In sperm cells,
555 the mitochondrion resides at the base of the flagellum to provide energy for flagellar
556 movement[21]. While we observed close apposition of the mitochondria with axonemal
557 tubulin in some activated males using light microscopy (Fig. S4), this was not consistently
558 observed in all males, and we lack the resolution to prove real association. Another
559 explanation could be that the parasite undergoes a form of mitophagy as a source for
560 proteins, lipids, and nucleotides required for the rapid nuclear division and microgamete
561 formation. Even though mitophagy has not been studied in *Plasmodium*, some homologues
562 of the general autophagy pathway have been identified[32]. Autophagy as a survival
563 mechanism was described for *P. falciparum* and *T. gondii* under starvation conditions[33,34]. In
564 *T. gondii*, the fragmentation of the mitochondrion was reversed by using the established
565 autophagy inhibitor 3-methyl adenine[33]. Alternatively, the distribution of the mitochondria
566 could merely be a consequence of the nuclear expansion in the cell.
567

568 Mitochondrial dynamics during mosquito stages is poorly understood and to our knowledge
569 studies have thus far been restricted to *P. berghei*[16,22,23,35]. Here, we visualized the
570 mitochondrion in *P. falciparum* during mosquito stages for the first time. In early oocyst
571 stages, the mitochondrion resembles the extensively branched network from asexual blood-
572 stage schizonts. During oocyst development, the mitochondrial network organizes into
573 multiple MOCs that resemble the cartwheel structure observed in asexual blood stages. In *P.*
574 *berghei* liver-stage schizonts, a very similar mitochondrial organization was observed in sub-
575 compartments created by large membrane invaginations[11,36]. Similar sub-compartments are
576 present during oocyst development[36]. Based on apicoplast visualizations in *P. berghei* and
577 our observations of the formation of MOCs during oocyst stages, mitochondrial and
578 apicoplast dynamics in these sub-compartments in both oocyst and liver stages resemble
579 the dynamics of these organelles in blood-stage schizogony[11,37,38].
580
581 Although the use of new imaging techniques, such as expansion microscopy and 3D volume
582 EM, have revealed new insights in mitochondrial dynamics, many questions about the
583 timing and organization of mitochondrial division remained unanswered[10,31]. In an earlier
584 literature review, we proposed three possible mitochondrial division models: synchronous
585 fission, outside-in fission, or branching point fission[8]. Here, we used a new mitochondrial
586 marker and advanced imaging techniques, such as Airyscan confocal microscopy and FIB-
587 SEM, to reconstruct mitochondrial fission during schizogony, which allows us to propose a
588 new, detailed model for mitochondrial fission (Figure 8). In this model, we describe the
589 cartwheel orientation of the mitochondrion, its non-geometric 2^n division, the late timing of
590 division, and its association with the apicoplast. In other eukaryotic models, mitochondrial
591 fission is facilitated by adaptor proteins on the cytoplasmic side of the outer mitochondrial
592 membrane that recruit dynamin GTPases, which in turn oligomerize to form a constrictive
593 ring around the organelle[8]. *P. falciparum* harbors three dynamins, however, their role in
594 organelle division still needs to be confirmed. The only conserved adaptor protein in *P.*
595 *falciparum*, Fission 1 (Fis1), is dispensable in asexual blood stages precluding an essential
596 role in mitochondrial fission during schizogony[39]. Which proteins comprise the
597 mitochondrial division machinery in *P. falciparum* remains to be explored. The specific
598 location at the entrance of the developing merozoite during mid-segmentation stages could
599 suggest that the bulbous invagination structures, or bulins, could play a role in
600 mitochondrial fission or in the distribution of certain components, e.g. mitochondrial DNA,
601 to the branches of the mitochondrial cartwheel structure that enter the merozoite.
602 However, in earlier stages, bulins are also found at branching points or in continuous parts
603 of the mitochondrion and apicoplast, perhaps suggesting possible roles in more general
604 membrane remodeling of the organellar network.
605
606 The use of volume EM provided the resolution required to verify our fluorescence-based
607 mitochondrial fission model while simultaneously shedding light on the division of the
608 second endosymbiotic organelle, the apicoplast. The apicoplast likely utilizes a similar
609 dynamin-based division machinery as the mitochondrion[8]. As the timing of the apicoplast
610 division precedes that of the mitochondrion, it is even conceivable that (parts of) the same
611 machinery may be reused. The apicoplast divides when nuclear division is still ongoing and
612 merozoite segmentation has just started (Figure 8). Similar to the mitochondrion, its division
613 does not happen in a geometric 2^n progression, but different sized apicoplast fragments are
614 observed in a mid-division stage. The specific types of membrane contact between both

615 endosymbiotic organelles, whether they are direct physical contacts, membrane fusion or
616 tethering, may vary and remain to be explored. The timing and orientation of these
617 organelle appositions, suggest a potential role of the apicoplast in mitochondrial
618 segregation. However, doxycycline treated parasites, that have lost their apicoplast and are
619 chemically rescued by isopentenyl pyrophosphate supplementation, can still produce viable
620 merozoites, suggesting that association with the apicoplast is not essential for mitochondrial
621 segregation[40].
622
623 We also observed CPs, the *P. falciparum* analogue of the centrosome, which function as
624 microtubule organizing centers and are important for mitosis and cell cycle regulation[41,42]. In
625 *T. gondii*, the centrosome associates with the apicoplast and ensures correct segregation of
626 the organelle during daughter cell formation[43,44]. Recent expansion microscopy data
627 suggested interaction of the CP with both the apicoplast and the mitochondrion in *P.*
628 *falciparum*[31]. From the onset of IMC and rhoptry formation, we observed close apposition of
629 the CPs and apicoplast, but not the mitochondrion (Figure 8). This CP-apicoplast association
630 continues during and after apicoplast division, indicating a role of the CPs in apicoplast
631 segregation. The initial absence of CP-apicoplast association and the later association of two
632 CPs from one nucleus with separate apicoplast branches suggests an active recruitment
633 strategy. Motor proteins facilitate intracellular transport of organelles along the
634 cytoskeleton in multicellular eukaryotes. While dynein and kinesin facilitate organelle
635 transport along microtubules, myosin motor proteins transport organelles along actin
636 filaments to specific locations in the cell[45]. Previous studies have shown a critical role of F-
637 actin and myosin F in the inheritance of the apicoplast in *P. falciparum* and *T. gondii*[46–49]. In
638 *T. gondii* parasites that lack myosin F, the apicoplast fails to associate with centrosomes[50].
639 Therefore, we hypothesize that myosin facilitates recruitment of the apicoplast branches
640 over the actin filaments to the CPs. Although the mitochondrion is close to the CPs in late
641 segmentation stages, the distance is always significantly bigger than the apicoplast-CP
642 distance. Additionally, mitochondrial branches reach much further into the merozoites
643 when fully segmented, compared to the apicoplast. Furthermore, conditional knockout of
644 *Pf*ACT1 (actin-1) did not alter mitochondrial morphology in asexual blood-stage
645 schizogony[46]. Therefore, it remains questionable if the mitochondrial branches are recruited
646 to the CP via a similar mechanism as the apicoplast.
647
648 Volume EM is a powerful tool to study biological questions as it allows the visualization of
649 complex, connecting structures and gives spatial and cellular context. Here, we reused
650 available FIB-SEM data which contains sexual and asexual parasites from many different
651 stages. Future reinterrogation of the data could facilitate in answering other biological
652 questions that are beyond the scope of this paper, such as rhoptry biogenesis and
653 development of the apical complex.
654
655 In this study, we have developed a reporter parasite line harboring a fluorescent
656 mitochondrial marker, integrated in a new genomic locus that can be used for mitochondrial
657 visualization in blood and mosquito stages. This allowed us to visualize mitochondrial
658 division in great detail and describe the relative timing and events of mitochondrial fission
659 and segregation using high-resolution confocal microscopy and FIB-SEM image analysis.
660 Combined with new insights in apicoplast division, mitochondrial and apicoplast interaction,
661 and association of the apicoplast with the CP during schizogony, this allowed us to propose

662 a new, detailed model of apicoplast and mitochondrial division during schizogony. These
663 findings pave the path for more targeted approaches to study the mechanism of
664 mitochondrial and apicoplast division and segregation.

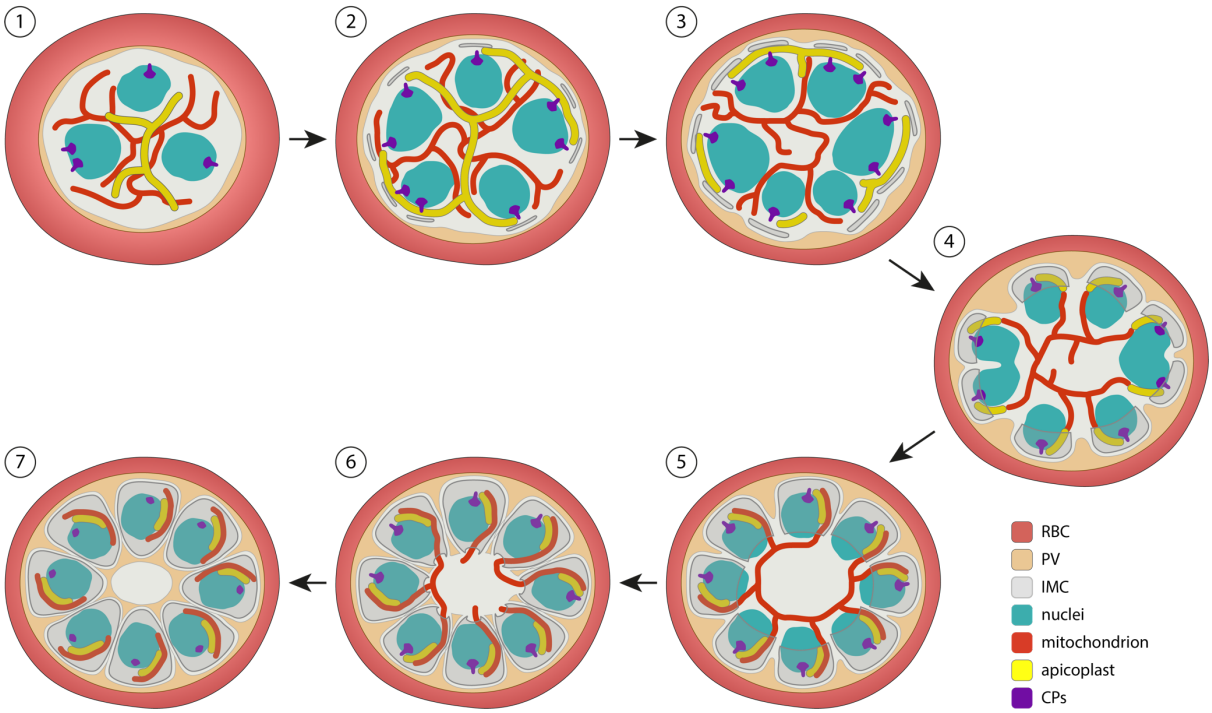

Figure 8. Schematic model for mitochondrial and apicoplast division and segregation in* P. falciparum *during schizogony. *(1) Nuclear division is ongoing, while inner membrane complex (IMC) formation has not started and both the mitochondrion and apicoplast are branched networks. The apicoplast localizes more to the center of the cell, while the mitochondrion is stretched throughout the whole cell. (2) When IMC formation starts, the apicoplast branches associate with the centriolar plaques (CPs) at the periphery of the parasite. (3) The apicoplast divides in a non 2^n progression, while it keeps its interaction with the CPs. (4) When nuclear division is finishing, apicoplast division is completely finished. The apical end of the apicoplast fragments associate with the CPs, while mitochondrial branches associate with the basal end of the apicoplast fragments. (5) The IMC develops further and envelops large parts of the nuclei. The mitochondrion orients itself in a cartwheel structure, while its branches align with the apicoplast fragments. (6) IMC formation is almost finished, and just a small opening connects the merozoites to the residual body. The mitochondrion divides in a non 2^n progression. The apicoplast still associates with the CPs and aligns with mitochondrial branches/fragments. (7) Merozoite segmentation is complete, the apicoplast loses its clear association with the CPs since they become smaller and do not have a clear extra nuclear compartment anymore. The mitochondrion is fully divided and still aligns with the apicoplast. Red blood cell (RBC), parasitophorous vacuole (PV).*

683 ## Materials and Methods

684 ***P. falciparum* culture and transfections**

685 *P. falciparum* NF54 and MitoSIL7 parasites were cultured in RPMI1640 medium
686 supplemented with 25 mM HEPES, 10% human type A serum and 25 mM $NaHCO_3$ (complete
687 medium). Parasites were cultured in 5% human RBCs type O (Sanquin, the Netherlands) at
688 37 °C with 3 % O_2 and 4 % CO_2. For transfection, 60 µg of HDR plasmid was linearized by
689 overnight digestion, precipitated, and transfected with 60 µg Cas9 plasmid using ring
690 transfection[51,52]. Briefly, a ring-stage sorbitol synchronized parasite culture was transfected
691 with the plasmids by electroporation (310 V, 950 µF). Five hours after transfection, parasites
692 were treated with 2.5 nM WR99210 for five days. Success of transfection was assessed by
693 integration PCR (Fig S1, Table S1).
694

695 **Plasmid constructs**

696 To generate the base SIL7 reporter plasmid (pRF0057) the 5' and 3' homology regions for
697 SIL7 were amplified from genomic NF54 DNA (Table S1) and cloned into the pBAT backbone
698 with NgoMIV and AleI (5') and BmgBI and AatII (3'). For the final MitoSIL7 repair plasmid,
699 first the mScarlet sequence was amplified from p1.2RhopH3-HA-mScarlet (a kind gift from
700 Prof. Alan Cowman) (Table S1). The mScarlet sequence was cloned into pRF0077 (empty
701 tagging plasmid with PBANKA_142660 bidirectional 3'UTR) with AflII and EcoRI restriction
702 sites, generating pRF0078 intermediate plasmid. The HSP70-3 promotor (prom) and
703 targeting sequence (t.s.) sequence was cloned into pRF0078 with EcoRI and NheI restriction
704 sites, generating pRF0079 intermediate plasmid. The whole mitochondrial marker (HSP70-3
705 prom + t.s. + mScarlet) was cloned from pRF0079 into pRF0057 with EcoRI and AflII
706 restriction sites, generating pRF0191, the final repair plasmid. CRISPR/Cas9 guide plasmids
707 targeting two different sites in the SIL7 region were generated. Guide oligonucleotides were
708 annealed and cloned into pMLB626 plasmid (a kind gift from Marcus Lee) using BbsI
709 restriction enzyme, generating the two final guide plasmids (Table S1).
710

711 **Growth assay**

712 NF54 WT and MitoSIL7 parasites were synchronized using 63% Percoll centrifugation. Late-
713 stage parasites were isolated from the Percoll gradient and added to fresh RBCs. Four hours
714 later, a 5% sorbitol synchronization was performed, which allowed only young rings that just
715 invaded a new RBC to survive. Ring stage parasites were counted and three independent
716 cultures of 0.05% parasitemia were set up for each parasite line. Every 24 hours, 10 µl
717 culture was taken and fixed in 100 µl 0.25% glutaraldehyde in PBS up until day 5. To prevent
718 overgrowth, parasite cultures were cut back 1/50 after samples were taken on day 3. Before
719 readout, fixative was taken of, and parasite DNA was stained with 1:10,000 SYBR Green in
720 PBS. Parasitemia was determined by measuring SYBR Green positive cells with a Cytoflex
721 flow cytometer (Beckman Coulter Cytoflex) using the 488 nm laser. Final parasitemia of day
722 4 and 5 was adjusted for the 1/50 dilution factor, explaining why final parasitemia can reach
723 more than 100%.
724

725 **Immunofluorescence assays**

726 IFAs were performed on asexual and sexual blood-stage parasites, using the same fixation
727 and staining protocols. Asexual blood-stage parasites were usually synchronized with 5%
728 sorbitol to get them in the preferred stage for the IFAs. For tight synchronization, late-stage
729 parasites were isolated with 63% Percoll centrifugation and added to fresh RBCs. Four hours

730 later, a 5% sorbitol was performed to select for young rings. Parasites were settled on a
731 poly-L-lysine coated coverslip for 20 min at 37 C. Parasites were fixed (4% EM-grade
732 paraformaldehyde, 0,0075% EM-grade glutaraldehyde in PBS) for 20 min and permeabilized
733 with 0.1% Triton X-100 for 10 min. Samples were blocked with 3% bovine serum albumin
734 (BSA) (Sigma-Aldrich) in PBS for 1 h. Primary and secondary antibody incubations were
735 performed for 1 h in 3% BSA. The nucleus was visualized by staining with 1 µM DAPI in PBS
736 for 1 h. PBS washes were performed between different steps. Parasites were mounted with
737 Vectashield (Vector Laboratories). Images were taken with a Zeiss LSM880 or LSM900
738 Airyscan microscope with 63x oil objective with 405, 488, 561, 633 nm excitations. Images
739 were Airyscan processed before analysis with FIJI software. MitoTracker stainings (including
740 MitoTracker™ Orange CMTMRos, Red CMXRos, Deep Red FM, all from ThermoFisher) were
741 done before settling and fixation by incubation of the parasites with 100 nM MitoTracker for
742 30 minutes at 37 °C, followed by a wash with complete media. The IMC protein GAP45 was
743 labeled using the anti-GAP45 rabbit antibody (1:5000) (a kind gift from Julian Rayner) and
744 goat anti-rabbit AlexaFluor 488 antibody (1:500, Invitrogen). Alfa-tubulin was labeled with
745 an anti-alfa tubulin mouse antibody (1.500, Thermofisher) and chicken anti-mouse
746 AlexaFluor 488 antibody (1:400, Invitrogen).
747
748 **Gametocyte generation and mosquito feeds**
749 Gametocyte cultures were maintained in a semi-automatic culturing system with media
750 changes twice a day[53]. MitoRed gametocytes used for imaging were induced by Albumax
751 supplementation. A mixed asexual culture of 1% was set up and cultured in medium
752 supplemented with 2.5% Albumax II (Thermo Fisher Scientific™) without human serum for
753 four days. After four days, parasites were cultured in complete medium again for further
754 gametocyte development. For mosquito feeding, MitoRed gametocytes were stress induced
755 through asexual overgrowing. A mixed asexual culture of 1% was set up and cultured for 2
756 weeks. At day 15 after gametocyte induction, gametocytes were fed to *Anopheles stephensi*
757 mosquitoes (Sind-Kasur Nijmegen strain)[54]. 24 hours after feeding, several mosquitoes were
758 dissected, and blood bolus was obtained for live imaging of ookinetes.
759
760 **Live imaging of asexual blood-stage parasites**
761 Sorbitol-synchronized MitoRed or NF54 schizonts were stained with 0.5 µg/ml Hoechst
762 33342 (Invitrogen, H3570) for 30 minutes at 37 °C for nuclear staining. MitoTracker
763 stainings (including MitoTracker™ Orange CMTMRos, Red CMXRos, Deep Red FM,
764 Rhodamin123, all from ThermoFisher) were done by incubation of the parasites with 100
765 nM MitoTracker or 1 µg/ml Rhodamin123 for 30 minutes at 37 °C, followed by a wash with
766 complete medium. Stained parasites were diluted 1:40 in complete medium and settled for
767 20 minutes at 37 °C in a poly-L-lysine coated µ-slide 8 well imaging chamber (Ibidi).
768 Unbound cells were washed away with phenol red free complete medium, in which cells
769 were also kept during imaging. Parasites were imaged on a Zeiss LSM880 Airyscan
770 microscope with 37 °C heated stage table and 63x oil objective. Images were Airyscan
771 processed before analysis with FIJI software.
772
773 **Live imaging of mosquito stage parasites**
774 Ookinetes were obtained from the blood bolus of infected mosquitoes 24 hours after
775 feeding. Ookinetes were stained by mouse monoclonal anti-*Pf*s25 conjugated antibody
776 (made in house, final concentration 15µg/ml). Stained sample was applied on a glass slide

and covert with a glass coverslip. The sample was immediately imaged on a Zeiss LSM880 Airyscan microscope with 63x oil objective. Mosquito midguts were dissected at day 7, 10, and 13 after infection and put on a glass slide in PBS covert with a glass coverslip. Samples were imaged immediately on Zeiss LSM880 or LSM900 microscope with 63x oil objective. Oocysts were identified based on their fluorescent mitochondrion and round shape in the brightfield channel. All images were Airyscan processed before analysis with FIJI software. 3D segmentations and visualizations were done by manual thresholding of the fluorescent signal in Arivis 4D vision software. Salivary glands were dissected on day 13, 16 and 21 after infection and stained with mouse monoclonal anti-CSP conjugated antibody (made in house, final concentration 1µg/ml). Stained glands were applied on a glass slide and covert with a glass coverslip. Samples were imaged on a Zeiss Axioscope A1 microscope with AxioCam ICc1.

FIB-SEM image analysis

FIB-SEM image stacks were reused from Evers *et al.*[19]. For these stacks, gametocyte-induced iGP2 parasite cultures were MACS purified. During this process many late-stage asexual parasites in these cultures were co-purified and fixed in the agarose blocks used for FIB-SEM imaging. Detailed sample preparation and FIB-SEM imaging methods are described in Evers *et al.*[19]. All image processing, visualizations and analysis was done in ORS Dragonfly software (2022.2). Segmentations were done by either manual segmentation or deep learning-based segmentation. Deep learning-based segmentations were manually reviewed and corrected when necessary. 3D renderings of segmented regions were converted to triangle meshes for visualization.

Acknowledgements

We thank members from the molecular malaria research group for the discussions. We also thank Aniek Garritsen for her contributions to the generation of the SIL plasmids. We do greatly appreciate the help from Chiara Andolina and Nicholas Proellochs with mosquito experiments. We would like to thank Astrid Pouwelsen, Jolanda Klaassen, Laura Pelser-Posthumus, Saskia Mulder and Jacqueline Kuhnen for breeding of mosquitoes and handling of the infected mosquitoes. We thank the Radboud Technology Center Microscopy, Radboud Technology Center flowcytometry, and Radboudumc Electron Microscopy Center for the use of their facilities. We are grateful to Alan Cowman for sharing the p1.2RhopH3-HA-mScarlet plasmid and Julian Rayner for sharing the anti-GAP45 antibody. J.M.J.V. is supported by an individual Radboudumc Master-PhD grant, C.B. by a PhD fellowship from the Radboud Institute for Molecular Life Sciences, Radboudumc (RIMLS018-009b), F.E. and T.W.A.K. were supported by the Netherlands Organisation for Scientific Research (NWO-VIDI 864.13.009), A.B.V. is supported by an NIH grant (R01 AI028398).

References

1. WHO. *World malaria report 2022*. (2022).
2. Vaidya, A. B. & Mather, M. W. Mitochondrial evolution and functions in malaria parasites. *Annu. Rev. Microbiol.* **63**, 249–267 (2009).
3. Painter, H. J., Morrisey, J. M., Mather, M. W. & Vaidya, A. B. Specific role of mitochondrial electron transport in blood-stage Plasmodium falciparum. *Nature* **446**, 88–91 (2007).
4. Ke, H. *et al.* Genetic investigation of tricarboxylic acid metabolism during the Plasmodium falciparum life cycle. *Cell Rep.* **11**, 164–174 (2015).
5. Evers, F. *et al.* Composition and stage dynamics of mitochondrial complexes in Plasmodium falciparum. *Nat. Commun.* **12**, 3820 (2021).
6. Lamb, I. M., Okoye, I. C., Mather, M. W. & Vaidya, A. B. Unique Properties of Apicomplexan Mitochondria. *Annu. Rev. Microbiol.* **77**, 541–560 (2023).
7. Goodman, C. D., Buchanan, H. D. & McFadden, G. I. Is the Mitochondrion a Good Malaria Drug Target? *Trends Parasitol.* **33**, 185–193 (2017).
8. Verhoef, J. M. J., Meissner, M. & Kooij, T. W. A. Organelle dynamics in apicomplexan parasites. *MBio* **12**, (2021).
9. van Dooren, G. G. *et al.* Development of the endoplasmic reticulum, mitochondrion and apicoplast during the asexual life cycle of Plasmodium falciparum. *Mol. Microbiol.* **57**, 405–419 (2005).
10. Rudlaff, R. M., Kraemer, S., Marshman, J. & Dvorin, J. D. Three-dimensional ultrastructure of Plasmodium falciparum throughout cytokinesis. *PLoS Pathog.* **16**, e1008587 (2020).
11. Stanway, R. R. *et al.* Organelle segregation into Plasmodium liver stage merozoites. *Cell. Microbiol.* **13**, 1768–1782 (2011).
12. Linzke, M. *et al.* Live and Let Dye: Visualizing the Cellular Compartments of the Malaria Parasite Plasmodium falciparum. *Cytom. Part A* **97**, 694–705 (2020).
13. Painter, H. J., Morrisey, J. M. & Vaidya, A. B. Mitochondrial electron transport inhibition and viability of intraerythrocytic Plasmodium falciparum. *Antimicrob. Agents Chemother.* **54**, 5281–5287 (2010).
14. Joanny, F., Held, J. & Mordmüller, B. In Vitro activity of fluorescent dyes against asexual blood stages of Plasmodium falciparum. *Antimicrob. Agents Chemother.* **56**, 5982–5985 (2012).
15. Gebru, T., Mordmüller, B. & Heldb, J. Effect of fluorescent dyes on in vitro-differentiated, late-stage plasmodium falciparum gametocytes. *Antimicrob. Agents Chemother.* **58**, 7398–7404 (2014).
16. Matz, J. M., Goosmann, C., Matuschewski, K. & Kooij, T. W. A. An Unusual Prohibitin Regulates Malaria Parasite Mitochondrial Membrane Potential. *Cell Rep.* **23**, 756–767 (2018).
17. Esveld, S. L. Van *et al.* A Prioritized and Validated Resource of Mitochondrial Proteins in Plasmodium Identifies Unique Biology. *mSphere* **6**, e00614-21 (2021).
18. Kooij, T. W. A., Rauch, M. M. & Matuschewski, K. Expansion of experimental genetics approaches for Plasmodium berghei with versatile transfection vectors. *Mol. Biochem. Parasitol.* **185**, 19–26 (2012).
19. Evers, F. *et al.* Comparative 3D ultrastructure of Plasmodium falciparum gametocytes. *bioRxiv* 2023.03.10.531920 (2023).
20. Billker, O. *et al.* Identification of xanthurenic acid as the putative inducer of malaria development in the mosquito. *Lett. to Nat.* **392**, 289–292 (1998).
21. Moraes, C. R. & Meyers, S. The sperm mitochondrion: Organelle of many functions. *Anim. Reprod. Sci.* **194**, 71–80 (2018).
22. Vega-Rodríguez, J. *et al.* The glutathione biosynthetic pathway of Plasmodium is essential for mosquito transmission. *PLoS Pathog.* **5**, 16–18 (2009).
23. Sturm, A., Mollard, V., Cozijnsen, A., Goodman, C. D. & McFadden, G. I. Mitochondrial ATP synthase is dispensable in blood-stage Plasmodium berghei rodent malaria but essential in the mosquito phase. *Proc. Natl. Acad. Sci. U. S. A.* **112**, 10216–10223 (2015).

24. Siciliano, G. *et al.* Critical Steps of Plasmodium falciparum Ookinete Maturation. *Front. Microbiol.* **11**, 1–9 (2020).
25. Ridzuan, M. A. M. *et al.* Subcellular location, phosphorylation and assembly into the motor complex of GAP45 during Plasmodium falciparum schizont development. *PLoS One* **7**, (2012).
26. Jones, M. L., Cottingham, C. & Rayner, J. C. Effects of calcium signaling on Plasmodium falciparum erythrocyte invasion and post-translational modification of gliding-associated protein 45 (PfGAP45). *Mol. Biochem. Parasitol.* **168**, 55–62 (2009).
27. Rudlaff, R. M., Kraemer, S., Streva, V. A. & Dvorin, J. D. An essential contractile ring protein controls cell division in Plasmodium falciparum. *Nat. Commun.* **10**, 2181 (2019).
28. Kono, M., Prusty, D., Parkinson, J. & Gilberger, T. W. The apicomplexan inner membrane complex. *Front. Biosci.* **18**, 982–992 (2013).
29. Voß, Y., Klaus, S., Guizetti, J. & Ganter, M. Plasmodium schizogony, a chronology of the parasite's cell cycle in the blood stage. *PLoS Pathog.* **19**, 1–21 (2023).
30. Gerald, N., Mahajan, B. & Kumar, S. Mitosis in the human malaria parasite Plasmodium falciparum. *Eukaryot. Cell* **10**, 474–482 (2011).
31. Liffner, B. *et al.* Atlas of Plasmodium falciparum intraerythrocytic development using expansion microscopy. *Elife* 1–39 (2023) doi:10.1101/2023.03.22.533773.
32. Hain, A. U. P. & Bosch, J. Autophagy in Plasmodium, a multifunctional pathway? *Comput. Struct. Biotechnol. J.* **8**, e201308002 (2013).
33. Ghosh, D., Walton, J. L., Roepe, P. D. & Sinai, A. P. Autophagy is a cell death mechanism in Toxoplasma gondii Debasish. *Cell. Microbiol.* **23**, 1–7 (2012).
34. Joy, S. *et al.* Basal and starvation-induced autophagy mediates parasite survival during intraerythrocytic stages of Plasmodium falciparum. *Cell Death Discov.* **4**, (2018).
35. Saeed, S., Tremp, A. Z., Sharma, V., Lasonder, E. & Dessens, J. T. NAD (P) transhydrogenase has vital non-mitochondrial functions in malaria parasite transmission . *EMBO Rep.* **21**, 1–11 (2020).
36. Burda, P.-C. *et al.* A Plasmodium plasma membrane reporter reveals membrane dynamics by live-cell microscopy. *Sci. Rep.* **7**, 9740 (2017).
37. Stanway, R. R., Witt, T., Zobiak, B., Aepfelbacher, M. & Heussler, V. T. GFP-targeting allows visualization of the apicoplast throughout the life cycle of live malaria parasites. *Biol. cell* **101**, 415–430 (2009).
38. Roques, M., Bindschedler, A., Beyeler, R. & Heussler, V. T. Same, same but different: Exploring Plasmodium cell division during liver stage development. *PLoS Pathog.* **19**, 1–22 (2023).
39. Maruthi, M., Ling, L., Zhou, J. & Ke, H. Dispensable role of mitochondrial fission protein 1 (Fis1) in the erythrocytic development of Plasmodium falciparum. *mSphere* **5**, e00579-20 (2020).
40. Yeh, E. & DeRisi, J. L. Chemical rescue of malaria parasites lacking an apicoplast defines organelle function in blood-stage Plasmodium falciparum. *PLoS Biol.* **9**, e1001138 (2011).
41. Arnot, D. E., Ronander, E. & Bengtsson, D. C. The progression of the intra-erythrocytic cell cycle of Plasmodium falciparum and the role of the centriolar plaques in asynchronous mitotic division during schizogony. *Int. J. Parasitol.* **41**, 71–80 (2011).
42. Simon, C. S. *et al.* An extended DNA-free intranuclear compartment organizes centrosome microtubules in malaria parasites. *Life Sci. Alliance* **4**, 1–15 (2021).
43. Striepen, B. *et al.* The plastid of Toxoplasma gondii is divided by association with the centrosomes. *J. Cell Biol.* **151**, 1423–1434 (2000).
44. van Dooren, G. G. *et al.* A novel dynamin-related protein has been recruited for apicoplast fission in Toxoplasma gondii. *Curr. Biol.* **19**, 267–276 (2009).
45. Frederick, R. L. & Shaw, J. M. Moving mitochondria: Establishing distribution of an essential organelle. *Traffic* **8**, 1668–1675 (2007).
46. Das, S., Lemgruber, L., Tay, C. L., Baum, J. & Meissner, M. Multiple essential functions of

Plasmodium falciparum actin-1 during malaria blood-stage development. *BMC Biol.* **15**, 1–16 (2017).

47. Periz, J. *et al.* Toxoplasma gondii F-actin forms an extensive filamentous network required for material exchange and parasite maturation. *Elife* **6**, e24119 (2017).
48. Stortz, J. F. *et al.* Formin-2 drives polymerisation of actin filaments enabling segregation of apicoplasts and cytokinesis in Plasmodium Falciparum. *Elife* **8**, 1–34 (2019).
49. Jacot, D., Daher, W. & Soldati-Favre, D. Toxoplasma gondii myosin F, an essential motor for centrosomes positioning and apicoplast inheritance. *EMBO J.* **32**, 1702–1716 (2013).
50. Devarakonda, P. M., Sarmiento, V. & Heaslip, A. T. F-actin and myosin F control apicoplast elongation dynamics which drive apicoplast-centrosome association in Toxoplasma gondii. *MBio* **14**, (2023).
51. Wu, Y., Sifri, C. D., Lei, H. H., Su, X. Z. & Wellems, T. E. Transfection of Plasmodium falciparum within human red blood cells. *Proc. Natl. Acad. Sci. U. S. A.* **92**, 973–977 (1995).
52. Crabb, B. S. & Cowman, A. F. Characterization of promoters and stable transfection by homologous and nonhomologous recombination in Plasmodium falciparum. *Proc. Natl. Acad. Sci. U. S. A.* **93**, 7289–7294 (1996).
53. Ponnudurai, T., Lensen, A. H. W., Meis, J. F. G. M. & Meuwissen, J. H. E. Synchronization of Plasmodium falciparum gametocytes using an automated suspension culture system. *Parasitology* **93**, 263–274 (1986).
54. Feldmann, A. M. & Ponnudurai, T. Selection of Anopheles stephensi for refractoriness and susceptibility to Plasmodium falciparum. *Med. Vet. Entomol.* **3**, 41–52 (1989).